Electronic supplementary materials

For https://doi.org/10.1631/jzus.A2200198

Experimental and numerical study of seepage-induced suffusion under K_0 stress state

Tuo WANG[1,2], Feng-shou ZHANG[1,2], Pei WANG[3]

[1]*Key Laboratory of Geotechnical & Underground Engineering of Ministry of Education, Tongji University, Shanghai 200092, China*

[2]*Department of Geotechnical Engineering, College of Civil Engineering, Tongji University, Shanghai 200092, China*

[3]*Department of Civil and Environmental Engineering, The Hong Kong Polytechnic University, Kowloon, Hong Kong 999077, China*

S1 Dynamic fluid mesh algorithm

In the DEM model, the centroids of the coarse particles and the contact points between the walls and the coarse particles are used to generate the tetrahedral mesh by Delaunay triangulation (Blanco, 2015). The mesh is updated dynamically at predetermined time steps as the particles move during the calculation. This method provides a good representation of flow in gap-graded soils.

To obtain the porosity of each tetrahedron, the total volume of coarse and fine particles in each tetrahedron is calculated separately. For coarse particles, the volume of a tetrahedron embedded in the particle is first calculated. Then a volume correction factor is applied to the embedded tetrahedron in order to add a small additional volume near the spherical surface. For small particles, the total volume is recorded in the tetrahedron in which the particle centroid is located. Then the porosity, ϵ, is obtained as:

$$\epsilon = \frac{V_{\text{tet}} - V_{\text{coarse}} - V_{\text{fine}}}{V_{\text{tet}}} \tag{S1}$$

where V_{tet} is the volume of the tetrahedron mesh, V_{coarse} and V_{fine} represent the volume of

the tetrahedron embedded in coarse and fine particles, respectively. Permeability is obtained by using the Konzeny-Carman equation (Bear, 1972),

$$k = \frac{d_{\mathrm{m}}^2}{180}\frac{\epsilon^3}{(1-\epsilon)^2} \tag{S2}$$

where d_m is the average diameter of fine particles in the mesh.

Low Reynolds number fluid flow in porous medium is described by Darcy's law:

$$\boldsymbol{v} = -\frac{\boldsymbol{K}}{\mu\epsilon}\nabla p \tag{S3}$$

where, $\vec{v}$ is the fluid velocity, p is the fluid pressure, K is the matrix permeability, μ is the fluid dynamic viscosity, and ϵ is the matrix porosity.

The compressibility of the fluid is negligible, leading to the incompressibility condition:

$$\nabla \boldsymbol{v} = 0 \tag{S4}$$

A Laplace's equation (Eq. (S5)) is derived by combining Eqs. (S3) and (S4):

$$\nabla\left(\frac{\boldsymbol{K}}{\mu\epsilon}\nabla p\right) = 0 \tag{S5}$$

This equation is solved for piece-wise constant pressure over the fluid elements, using the *fipy* solver, which is a partial differential equation (PDE) solver (Silpa-Anan and Hartley, 2008). Given the boundary conditions, the pressure in each element can be solved. The fluid velocity on each element face can be solved by using Darcy's law, and the fluid velocity at the element centre is defined by the following interpolation scheme:

$$v_{i,i=1,2,3} = \frac{\sum_{j=1}^{4} n_{ji} v_{ji} S_j}{\sum_{j=1}^{4} n_{ji} S_j} \tag{S6}$$

where v_i is the fluid velocity in the i-direction of mesh center, S_j is the area of each element face, and n_{ji} is the vector in the i-direction of normal vector of surface j.

The hydro-mechanical forces on coarse and fine particles are calculated separately. For coarse particles, the force exerted on a particle from a single fluid element is calculated by multiplying the fluid pressure by the surface area of the coarse particle contained in the fluid element. The resultant force exerted by the fluid on the coarse particle can be written as:

$$\boldsymbol{f}_c = \sum_i P_i S_i \tag{S7}$$

where P_i is the pressure and S_i is the surface area of the particle in the fluid mesh.

For small particles, the total force exerted by the fluid on the particle is the sum of the drag force and the buoyancy force:

$$\boldsymbol{f}_f = \boldsymbol{f}_d + \frac{4}{3}\pi r^3 \rho_f \boldsymbol{g} \tag{S8}$$

where $\boldsymbol{f}_f$ is the total force applied by the fluid, and $\boldsymbol{f}_d$ is the drag force applied by the fluid, which can be expressed as:

$$\boldsymbol{f}_d = \frac{4}{3}\pi r^3 \frac{\boldsymbol{f}_b}{(1-\epsilon)} \tag{S9}$$

where *r* is the particle radius, $\boldsymbol{f}_b$ is the drag force per unit volume in the fluid mesh the particle occupies, and ϵ is the porosity.

The drag force that particles exert on the fluid in each fluid mesh is defined as:

$$\boldsymbol{f}_b = \beta \boldsymbol{U} \tag{S10}$$

where $\boldsymbol{f}_b$ is the drag force per unit volume, β is a coefficient, and $\vec{U}$ is the average relative velocity between the particles and the fluid, defined as:

$$\boldsymbol{U} = \overline{\boldsymbol{u}} - \boldsymbol{v} \tag{S11}$$

where $\vec{v}$ is the fluid velocity, and $\boldsymbol{u}$ is the average velocity of all particles in a given fluid mesh, defined as:

$$\overline{\boldsymbol{u}} = \frac{1}{N}\sum_j \boldsymbol{u}_j \tag{S12}$$

where the sum is over all particles that exist in the fluid mesh.

The coefficient β is calculated in two ways, depending on the porosity of the fluid mesh (Tsuji et al., 1993). For low porosity (ϵ<0.8), the relationship comes from observations of pressure drop in flow through porous media (Ergun, 1952):

$$\beta = \frac{(1-\epsilon)}{\bar{d}^2\epsilon^2}\left(150(1-\epsilon)\mu + 1.75\rho_f \bar{d}\left|\overline{\boldsymbol{U}}\right|\right) \qquad \epsilon < 0.8 \tag{S13}$$

where μ is the dynamic viscosity of the fluid, ρ_f is the density of the fluid, and $\overline{d}$ is the average diameter of the fine particles staying in the fluid mesh, which is defined as:

$$\overline{d} = \frac{1}{N}\sum_{j} d_{\mathrm{j}} \tag{S14}$$

where the sum is over all particles in a given fluid mesh.

For higher porosity ($\epsilon \geq 0.8$), β is derived from the corrected nonlinear drag force exerted on a spherical particle by a fluid (Wen and Yu., 1966):

$$\beta = \frac{4}{3} C_d \frac{|\boldsymbol{U}|\rho_f(1-\epsilon)}{\overline{d}\epsilon^{1.7}} \qquad \epsilon \geq 0.8 \tag{S15}$$

where C_d is a turbulent drag coefficient defined according to the particle Reynolds number:

$$C_d = \begin{cases} \dfrac{24(1+0.15R_{ep}^{0.687})}{R_{ep}} & R_{ep} < 1000 \\ 0.44 & R_{ep} \geq 1000 \end{cases} \tag{S16}$$

where,

$$R_{ep} = \frac{|\boldsymbol{U}|\rho_f \epsilon \overline{d}}{\mu} \tag{S17}$$

According to Eq. (S17), the Reynolds number is calculated. In this study, the Reynolds number is range 320 to 800, which is much lower than 2300. It indicates that the fluid is laminar flow.

S2 Rolling resistance contact model

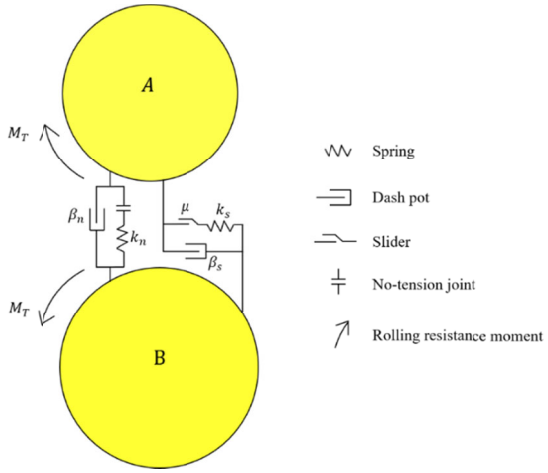

Figure S1 Schematic of rolling resistance linear model (Zhang et al., 2019).

The schematic of contact model is presented in Figure S1. The contact force is updated as

$$\boldsymbol{F}_c = \boldsymbol{F}^l + \boldsymbol{F}^d \tag{S18}$$

where $\vec{F}^l$ is the linear force and $\boldsymbol{F}^d$ is the dashpot force.

The rolling resistance moment is shown as,

$$M_T = \boldsymbol{M}_T - k_r \Delta \boldsymbol{\theta}_b \tag{S19}$$

where $\Delta\theta_b$ is the relative bend-rotational increment. The rolling resistance stiffness is defined as,

$$k_r = k_s \bar{R}^2 \tag{S20}$$

where k_s is the shear stiffness and $\bar{R}$ is the effective contact radius between the two particles in contact, defined as

$$\frac{1}{\bar{R}} = \frac{1}{\bar{R}^A} + \frac{1}{\bar{R}^B} \tag{S21}$$

The rolling resistance is capped by a limiting torque defined as,

$$\boldsymbol{M}^* = \mu_r \bar{R} \boldsymbol{F}_n^l \tag{S22}$$

where $\boldsymbol{F}_n^l$ is the normal component of the linear force, and μ_r is the rolling resistance coefficient,

defined as the tangent of the maximum angle of a slope on which the rolling resistance toque counterbalances the torque produced by the gravity acting on the body.

The rolling resistance results in two types of energy partition: the rolling strain energy and rolling slip energy. The rolling strain energy is shown as,

$$E_{kr} = \frac{1}{2}\frac{\|\boldsymbol{M}_T\|^2}{k_r} \tag{S23}$$

The rolling slip energy has the following form:

$$E_{\mu r} = E_{\mu r} - \frac{1}{2}(\boldsymbol{M}_T^o + \boldsymbol{M}_T) \cdot \Delta\boldsymbol{\theta}_b^{\mu r} \tag{S24}$$

where $\boldsymbol{M}_T^o$ is the rolling resistance moment at the beginning of the time step, while $\Delta\boldsymbol{\theta}_b^{\mu r}$ is the slip component of the relative bend-rotational increment, defined as the different between $\Delta\theta_b$ and the elastic component of the relative bend-rotational increment $\Delta\boldsymbol{\theta}_b^k$,

$$\Delta\boldsymbol{\theta}_b^{\mu r} = \Delta\boldsymbol{\theta}_b - \Delta\boldsymbol{\theta}_b^k = \Delta\boldsymbol{\theta}_b - \frac{(\boldsymbol{M}_T - \boldsymbol{M}_T^o)}{k_r} \tag{S25}$$

Reference:

Bear, J., 1972. Dynamics of fluids in porous media. American Elsevier Pub. Co., New York.

Blanco, S.F., 2015. Learning SciPy for numerical and scientific computing, Packt Pub. Packt Publishing. https://doi.org/10.1017/CBO9781107415324.004

Ergun, S., 1952. Fluid flow through packed columns. Chem. Eng. Prog. 48, 89–94.

Nardelli, V., Coop, M.R., Andrade, J.E., Paccagnella, F., 2017. An experimental investigation of the micromechanics of Eglin sand. Powder Technol. 312, 166–174. https://doi.org/10.1016/j.powtec.2017.02.009

Silpa-Anan, C., Hartley, R., 2008. Optimised KD-trees for fast image descriptor matching, in: IEEE Conference on Computer Vision & Pattern Recognition. IEEE, Anchorage, Alaska, USA.

Tsuji, Y., Kawaguchi, T., Tanaka, T., 1993. Discrete particle simulation of two-dimensional fluidized bed. Powder Technol. 77, 79–87. https://doi.org/10.1016/0032-5910(93)85010-7

Wang, P., Yin, Z.-Y., Wang, Z.-Y., 2022. Micromechanical Investigation of Particle-Size Effect of Granular Materials in Biaxial Test with the Role of Particle Breakage. J. Eng. Mech. 148, 1–14. https://doi.org/10.1061/(asce)em.1943-7889.0002039

Wen, C.Y., Yu., Y.H., 1966. Mechanics of fluidization. Chem. Eng. Prog. Symp. Ser. 62, 100–111.

Zhang, F., Li, M., Peng, M., Chen, C., Zhang, L., 2019. Three-dimensional DEM Modeling of the Stress–strain Behavior for the Gap-graded Soils Subjected to Internal Erosion. Acta Geotech. 14, 487–503. https://doi.org/10.1007/s11440-018-0655-4